ELSEVIER

Journal of Nuclear Materials 245 (1997) 27–33

journal of nuclear materials

Experimental evidence of lithium migration out of an irradiated boron carbide material

D. Simeone [a,*], X. Deschanels [a], B. Berthier [b], C. Tessier [b]

[a] *Centre d'Etudes de Saclay, Laboratoire d'Etude des Matériaux Absorbants, F-91191 Gif-sur-Yvette cedex, France*
[b] *Centre d'Etudes de Saclay, Laboratoire Pierre Süe, CEA-CNRS, F-91191 Gif-sur-Yvette cedex, France*

Received 25 June 1996; accepted 16 December 1996

Abstract

The nuclear microprobe technique has been used to measure the ^{10}B and ^{7}Li profiles after thermal neutron irradiation of a boron carbide absorber. This technique allowed to obtain the ^{10}B, ^{11}B and ^{7}Li concentrations along the radius of the absorbing pellet. The ^{10}B measured distribution is used to calculate the spatial distribution of ^{7}Li if no migration out of the sample is expected. This result is compared to the ^{7}Li measured distribution. This comparison suggests that ^{7}Li atoms have migrated out of the sample with a loss of about 40% in the pellet. Some assumptions have been investigated in order to explain the main cause of the ^{7}Li migration. This lithium migration may increase significantly the boron carbide brittleness and may be important for the understanding of the boron carbide destruction mechanism under neutron irradiation.

1. Introduction

Control rods of pressurized water reactors (PWR) are used for neutron absorption during the control and the shut down of the generating plant. They are made of two kinds of absorber material: an alloy of silver indium and cadmium (Ag–In–Cd) and a ceramic material, boron carbide (B_4C). B_4C is the only material used in both fast breeder reactors (FBR) and pressurized water reactors (PWR) because of its neutron efficiency. A low neutron induced activity, a low cost and a high melting point make B_4C an attractive material.

Under neutron irradiation, the $^{10}B(n, \alpha)^{7}Li$ reaction induces a swelling of the control rod which reduces its lifetime. Many authors have shown the creation of He bubbles in the B_4C rods [1], but the effect of ^{7}Li atoms is not yet understood [2].

In order to investigate a possible migration of ^{7}Li out of the sample, we have measured the ^{7}Li, ^{10}B and ^{11}B concentrations along a radius of a rod. This has been performed using the nuclear reaction technique at the Pierre Süe Laboratory Microprobe facility [3].

Two ^{7}Li profiles have been obtained and compared, the first one from the experimental measurement of ^{7}Li, the second one deduced from the ^{10}B profile. The comparison of these two profiles of ^{7}Li along the radius of the pellet shows a lack of ^{7}Li atoms. A possible explanation of this lack of ^{7}Li is suggested.

2. Experimental details

2.1. Sample preparation

2.1.1. Material processing

Under thermal neutron irradiation and for an average number of 2×10^{21} captured neutrons per cm^3, usual boron carbide pellets are partially fragmented near their surface because of the high level of transmutation of ^{10}B in this area. Consequently, it is not possible to analyze this sample with the nuclear microprobe technique. To avoid such a problem, a composite material made of B_4C powder and an organic resin have been elaborated. The different

* Corresponding author. Fax: +33-1 69 08 90 82.

PII S0022-3115(96)00748-9

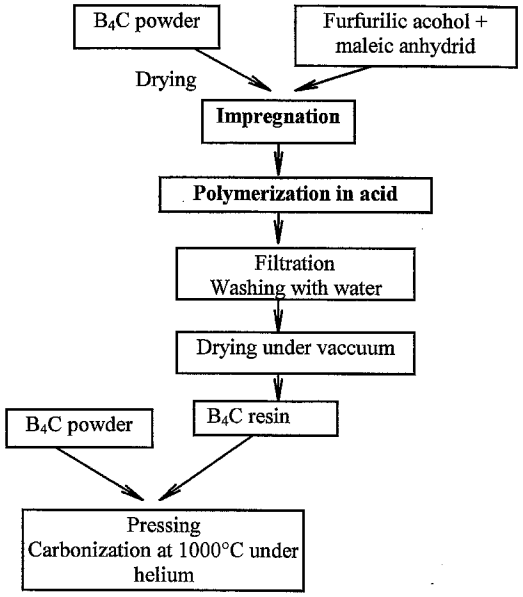

Fig. 1. Processing steps of B_4C/carbon pellet.

processing steps of this composite material are presented in Fig. 1.

Before the processing, the amount of resin in the initial powder was about 10 wt%. The mean grain size of the boron carbide powder is lower than 2 μm.

After the processing, the sample is composed of B_4C particles embedded in a carbonized resin. The observed porosity of the sample is about 25.8%. The open porosity volume is about 23.3% and the closed porosity volume is about 2.5%. This porosity is essentially localized in the carbonized resin (Fig. 2).

X-rays microanalysis (EDX) of the sample shows that boron and carbon images are quite similar. Only some carbon rich areas smaller than 10 μm^2 could be observed. These observations indicate a quite good homogenization of these elements during the processing. The analysis also shows the presence of small precipitates (< 10 μm^2) of magnesium boride and silicon oxide. Quantitative EDX analysis indicates that the sum of magnesium and silicon impurities is lower than 1.5 wt%.

2.1.2. Sample irradiation

The analyzed sample had an initial boron isotopic composition $N(^{10}B)/[N(^{10}B)+N(^{11}B)]$ equal to 20.8% (N(X) is the number of atoms of the chemical element X per volume unit). It was irradiated inside a capsule of quartz filled with ^4He. Two thermocouples measured the temperature at the surface of the sample during the irradiation. The temperature was about 780 K. The irradiation lasted 120 days with a thermal neutron flux of 3.0×10^{12} n cm^{-2} s^{-1}, and a fast neutron flux ($E_n > 1$ MeV) of 1.0×10^{14} n cm^{-2} s^{-1}. During the irradiation, a part of ^{10}B was transmuted into ^7Li and ^4He according to the fission reaction

$$n + {}^{10}B \rightarrow {}^{7}Li\ (0.83\ MeV) + {}^{4}He\ (1.48\ MeV).$$

A part of the produced ^7Li is transmuted into ^3H and ^4He by the reaction

$$n + {}^{7}Li \rightarrow n + {}^{3}H + {}^{4}He.$$

This last nuclear reaction occurs only under energetic neutrons bombardment ($E_n > 2.8$ MeV), with a cross section of about 0.4 b. Calculations have been done to estimate the ^7Li burn-up. This phenomenon is maximum near the pellet surface, but it is about four orders of magnitude smaller than the ^{10}B burn-up at the same position. The ^7Li burn-up can be neglected.

2.1.3. Sample preparation for microprobe analysis

For proton micro-beam analysis, an irradiated boron carbide cylinder with a radius R equal to 3.72 mm and a thickness of 2 mm has been polished with a patterned structure less than 1 μm in order to remove edge effects from scattered particles. Due to the ^7Li high solubility in water, a dry polishing with diamond abrasive powder has been done at room temperature. An epoxy resin, included under vacuum, was used to protect the pellet during the polishing and to avoid that many grains be pulled out because of the high porosity level of the pellet. The EDX analysis shows an excess of carbon near the epoxy resin

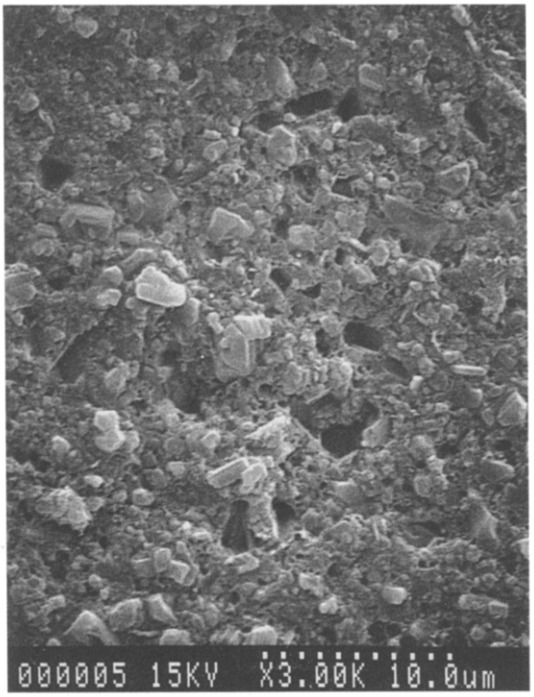

Fig. 2. Microstructural appearance of a polished section of the sample before neutron irradiation.

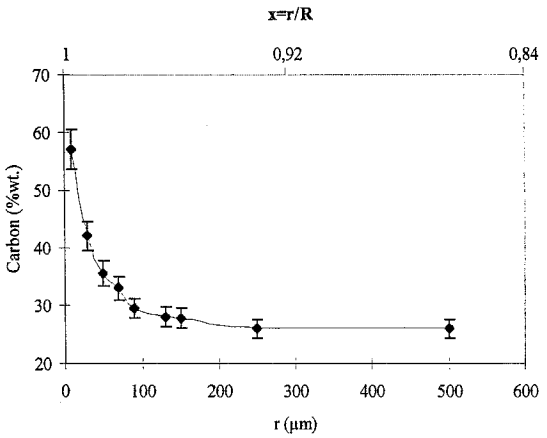

Fig. 3. Carbon profile at the resin–pellet interface. (x is the reduced abscissa from sample center and R is the radius of the cylinder.)

interface of the pellet (Fig. 3). This excess is due to the filling of the pellet porosity by the resin. This variation of carbon concentration induces some artifacts in the determination of the ^{7}Li and ^{10}B profiles near the interface of the sample, due to the variation of the stopping power.

2.2. Microprobe experiment

During neutron irradiation, the self-shielding of the pellet by the ^{10}B induces ^{7}Li and ^{10}B concentration profiles along the pellet radius. McMillan et al. [2] have already shown ^{7}Li profiles in pellets irradiated in FBR using the ^{7}Li(p, α) α nuclear reaction.

In the present work, ^{7}Li, ^{10}B and ^{11}B profiles have been measured by the following nuclear reactions:

$^{7}\mathrm{Li}(\mathrm{p}, \mathrm{p}'\gamma)^{7}\mathrm{Li}, \quad E_{\gamma} = 478\ \mathrm{keV},$

$^{10}\mathrm{B}(\mathrm{p}, \alpha\gamma)^{7}\mathrm{Be} \quad E_{\gamma} = 429\ \mathrm{keV},$

$^{11}\mathrm{B}(\mathrm{p}, \mathrm{p}'\gamma)^{11}\mathrm{B} \quad E_{\gamma} = 2125\ \mathrm{keV}.$

Two main advantages can be pointed out by using these reactions. First, they are induced simultaneously by the proton beam allowing concentration measurements at the same points in the pellet. Second, the counting rate is high enough to obtain the profiles along a pellet radius in a reasonable time. The proton beam energy, $E_{\mathrm{p}} = 3.2$ MeV, has been chosen to optimize the counting rate for the three nuclear reactions.

2.2.1. Microprobe description

The experimental arrangement is shown Fig. 4. The proton beam is delivered by an HF source and accelerated by a Van de Graaff accelerator. An analyzing magnet located at 3.5 m from the accelerator output allows to bend the beam into one of the available lines. The magnetic field is adjusted to choose the kind of beam particle and its energy.

The geometry of the micro-beam, spatial and angular dispersion is optimized by two slit systems 6 m apart. The beam is focused on the sample by a quadrupole doublet. The spot size depends on the experiment. It is obtained by adjusting the magnetic field in the doublet and the aperture of the slits.

The samples are mounted on a target holder fixed on a X–Y–Z–Θ Ultra High Precision Manipulator (U.H.P.M.). The U.H.P.M. allows a positioning of the sample with an accuracy of 0.5 μm.

The gamma photons emitted by the nuclear reactions are detected at 0° by a High Purity Germanium Detector (80% efficiency, 2.8 keV energy resolution).

The material presents an heterogeneous microstructure (porosity, secondary phase precipitates). For this reason, the beam size has been taken large enough, $15 \times 15\ \mu\mathrm{m}^2$, to average the measurement over the structure of the sample. Under these conditions, experiments performed with unirradiated B_4C sample provide ^{10}B and ^{11}B homogeneous concentrations in the composite pellet. These results have been used for normalization purposes in the analysis of the ^{10}B and ^{11}B profiles of the irradiated

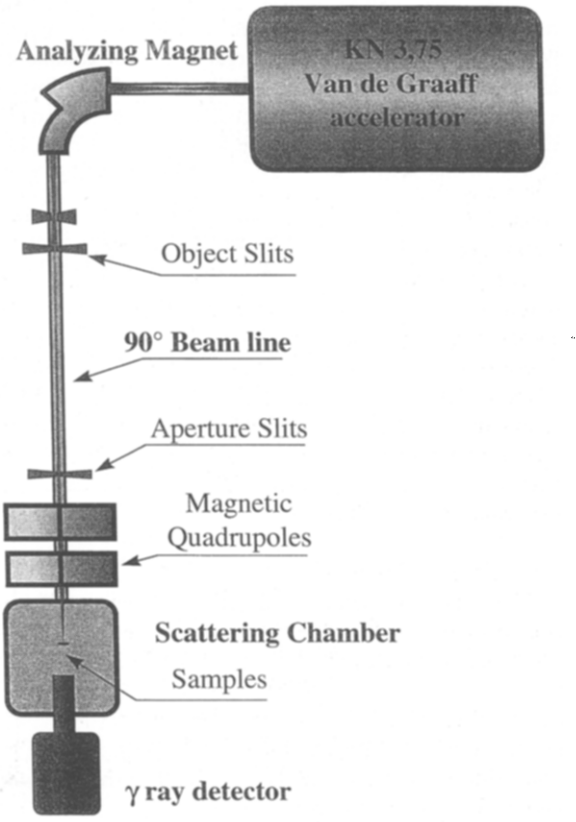

Fig. 4. Experimental arrangement to detect the γ-rays induced by the proton beam.

sample. The absorption of gamma photons by the samples has been estimated with a ^{152}Eu radioactive source. The differential absorption between the studied samples is less than 1%. It has been neglected in our analysis.

3. Experimental results

A typical energy spectrum is shown on Fig. 5. The number of counts in each gamma ray of interest is obtained by summing the contents of the channels which define the ray. A linear background is deduced to eliminate the Compton contribution of all the higher energy gamma rays.

The number of detected photons depends on the concentration of the analyzed elements (^{10}B, ^{11}B, ^{7}Li) according to the equation

$$N_\gamma(\mathrm{X},\ x,\ t_{\mathrm{irr}}) = kN(\mathrm{X},\ x,\ t_{\mathrm{irr}})N_\mathrm{p}\,\beta, \qquad (1)$$

where β is

$$\beta = \int_{E_\mathrm{c}}^{E_\mathrm{p}} \frac{\mathrm{d}\sigma}{\mathrm{d}\Omega}\frac{\mathrm{d}E}{(\mathrm{d}E/\mathrm{d}x)},$$

X is the studied element (^{7}Li, ^{10}B or ^{11}B); $N_\gamma(\mathrm{X},\ x,\ t_{\mathrm{irr}})$ is the number of collected photons at the irradiation duration t_{irr} and at the reduced abscissa $x = r/R$; k is the factor depending on the geometry and the detector efficiency; $N(\mathrm{X},\ x,\ t_{\mathrm{irr}})$ is the number of target atoms per volume unit at the irradiation duration t_{irr} and at the reduced abscissa $x = r/R$; N_p is the number of incident protons; $\mathrm{d}\sigma/\mathrm{d}\Omega$ is the cross-section of the reaction; $(\mathrm{d}E/\mathrm{d}x)$ is the stopping power of the matrix; E_p is beam energy (3.2 MeV); and E_c is cut off energy for the nuclear reaction.

The stopping power of the matrix, has been calculated according to the Ziegler and Bierzack formula [4] and the Bragg rules [5].

In order to simplify the reading of equations, we neglect the reduced abscissa x and the irradiation duration t_{irr}. But we must keep in mind that $N(\mathrm{X})$ depends also on x and t_{irr}.

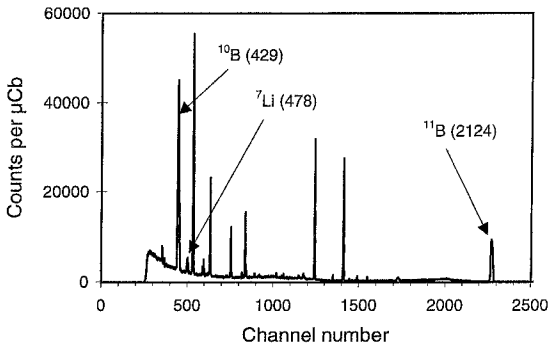

Fig. 5. γ-energy spectrum corresponding to the proton interaction with the pellet. The three lines of interest are identified.

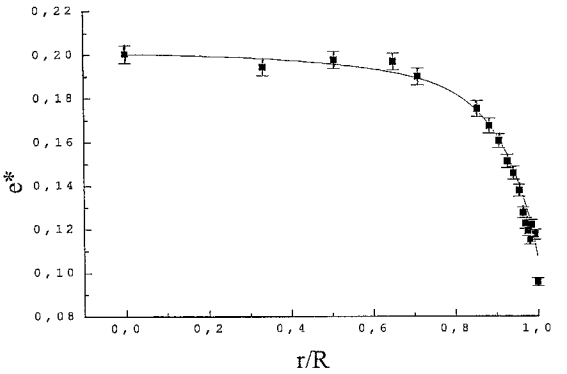

Fig. 6. Pellet ^{10}B ratio e^* along the radius of an irradiated B_4C pellet. (The star refers to the irradiated sample.)

3.1. ^{10}B profile

The ^{10}B concentration at a given point, $N(^{10}\mathrm{B})$ in Eq. (1), depends on four quantities.

The stopping power of the irradiated pellet is different of that of the unirradiated sample by a factor less than 0.5%. Doing the assumption that it is equal in both samples, we can simplify the calculation of the ^{10}B concentration by using the $N(^{10}\mathrm{B})/N(^{11}\mathrm{B})$ ratios in both, irradiated and unirradiated pellets. This method avoids to know the k, N_p and integral quantities. According to Eq. (1), we then obtain

$$\left[N(^{10}\mathrm{B})/N(^{11}\mathrm{B})\right]^* = \left[N(^{10}\mathrm{B})/N(^{11}\mathrm{B})\right] \left[N_\gamma(^{10}\mathrm{B})^*/N_\gamma(^{11}\mathrm{B})^*\right]\left[N_\gamma(^{11}\mathrm{B})/N_\gamma(^{10}\mathrm{B})\right]. \qquad (2)$$

The stars denote the irradiated sample.

The ratio, e^*, is obtained by the following relation:

$$e^* = \left[N(^{10}\mathrm{B})\right]^* / \left[N(^{10}\mathrm{B})^* + N(^{11}\mathrm{B})^*\right]. \qquad (3)$$

Fig. 6 shows this measured ratio e^* (black squares) along the reduced abscissa x (r/R ratio).

The full line represents the values of e^* deduced from a classical calculation including the neutron cross section on ^{10}B. As expected, the experimental values (black squares) decrease from the center to the surface of the boron carbide pellet, due to the neutron self-shielding of ^{10}B.

We observe a good agreement between the calculated values and the experimental measurements, except for points close to the interface pellet–epoxy resin ($x > 0.97$). The difference may come from a higher value of the stopping power due to the excess of carbon near the interface (cf. Section 2.1.3).

3.2. ^{7}Li profile

A reliable standard pellet of B_4C including a known concentration of ^{7}Li cannot be used to determine the ^{7}Li

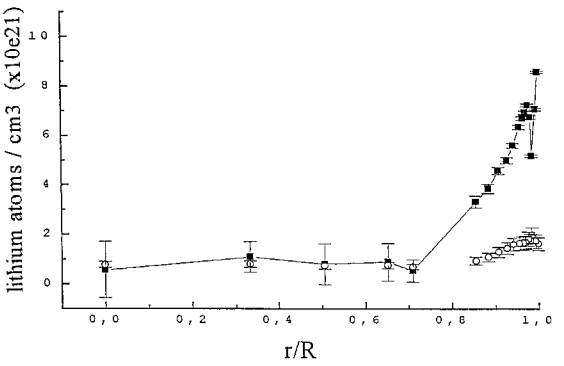

Fig. 7. ^{7}Li profiles along the radius of an irradiated B_4C. ■ – produced number of ^{7}Li atoms per volume unit along the radius of the irradiated sample. ○ – measured number of ^{7}Li atoms per volume unit along the radius of the irradiated sample.

profile according to Eq. (2). For this reason, reference measurements have been performed on a NBS standard composed of Si (25 at.%), Ca (4.5 at.%), Na (9.4 at.%), O (61.1 at.%) and Li (700 at.ppm). The NBS standard is a pellet with a radius of 3.5 mm and a thickness of 4 mm. NBS measurements were done using the same experimental arrangement as for boron carbide sample. The ^{7}Li concentration in the irradiated B_4C sample is then deduced from Eq. (4):

$$N(^{7}\mathrm{Li}) = N^{\mathrm{NBS}}(^{7}\mathrm{Li})\frac{N_{\gamma}(^{7}\mathrm{Li})}{N_{\gamma}^{\mathrm{NBS}}(^{7}\mathrm{Li})}\frac{\beta_{\mathrm{NBS}}}{\beta_{B_4C}}. \quad (4)$$

The cut-off energy of the ^{7}Li(p, p'γ)^{7}Li reaction, E_c, has been taken equal to 400 keV [6].

These results are shown on Fig. 7 as white circles.

From the knowledge of the ^{10}B experimental distribution, we have deduced the ^{7}Li expected profile. The number of ^{7}Li atoms generated in the irradiated pellet is given by the relation

$$N(^{7}\mathrm{Li}) = \frac{e - e^{*}}{e(1 - e^{*})}N(^{10}\mathrm{B}), \quad (5)$$

where e is the ratio $N(^{10}B)/[N(^{10}B) + N(^{11}B)]$ of the unirradiated boron carbide pellet. This ^{7}Li calculated profile is shown in Fig. 7 as black squares.

As expected, we show that the ^{7}Li profiles increase from the center to the edge of the sample. Near the center of the pellet, the calculations are in good agreement with the direct measurements but a large discrepancy is observed for $0.7 < x < 1$. This difference can be explained by ^{7}Li migration out of the pellet. The ^{7}Li profile deduced from the ^{10}B concentration provides an average value of $(2.44 \pm 0.2) \times 10^{21}$ atoms cm^{-3} whereas the average value of the experimental ^{7}Li measurement is $(1.4 \pm 0.15) \times 10^{21}$ atoms cm^{-3}. Approximately 40% of the ^{7}Li produced by the fission reaction migrates out of the pellet. A possible explanation of this phenomenon will be presented below.

A drop in ^{7}Li measured concentration is also observed for $x > 0.97$. This decrease may be an artifact partly caused by the excess of carbon discussed previously (cf. Section 2.1.3).

4. Discussion

To predict the lithium behavior in irradiated boron carbide pellets, a mechanism of lithium migration is presented. Two cases must be distinguished:

Migration of lithium atoms in the boron carbide bulk,

Migration of lithium atoms at the sample surface.

We study these cases separately.

4.1. Migration of lithium atoms in the boron carbide bulk

To explain this discrepancy of ^{7}Li atoms from the center to the surface of the pellet, a three step mechanism is proposed:

- Escape of the ^{7}Li atoms out of the boron carbide solid phase.
- Desorption of ^{7}Li at the boron carbide solid phase surface.
- Migration of ^{7}Li from the pores to the capsule free volume.

A schematic description is shown Fig. 8. This mechanism is detailed below.

4.1.1. Lithium escape out of the solid phase

The ^{10}B(n, α)^{7}Li reaction generates ^{7}Li atoms. These atoms may react with boron and carbon to create a chemical compound. They may also either precipitate as second phase in the sample inside the grain and at the grain boundary. A solubility of lithium atoms in the sample is also possible.

These three possibilities are discuss below.

The first possibility is the formation of lithium compounds [7]. Some authors have reported the formation of Li_2C_2 [8], LiB_{10} [9] and Li–C at high temperature (above

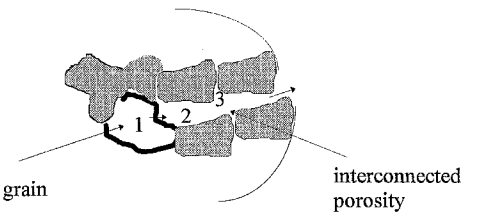

(1) diffusion of ^{7}Li in a boron carbide grain

(2) desorption at the grain surface

(3) migration of gaseous ^{7}Li in open pores of the sample

Fig. 8. Schematic of ^{7}Li transport in the boron carbide ceramic.

973 K) [10]. It is possible to calculate the temperature along the radius of the pellet taking into account the $^{10}B(n, \alpha)^{7}Li$ reaction nuclear heating. The temperature field is calculated using the well known heat equation in the steady state case by the following equation:

$$T(x) = T_{surface} + R^2 \int_x^1 \frac{dy}{y} \int_0^y \frac{P(u)u}{\lambda^{irr}} du; \quad (6)$$

x is the reduced abscissa, $T_{surface}$ is the temperature at the surface (793 K), and λ^{irr} is the thermal conductivity of the irradiated boron carbide pellet (6 W m^{-1} K^{-1}) [11].

$P(t)$ is the thermal source due to the nuclear heating (W m^{-3}). If we assume that this term is constant over the irradiation time, it can be written as follows:

$$P(x, t) = \frac{Q dN(Li, x, t_{irr})}{dt} \approx \frac{QN(Li, x, t_{irr})}{t_{irr}}; \quad (7)$$

Q is the energy of the transmutation reaction (2.7 MeV/atom), t_{irr} is the duration of the irradiation (120 days), $N(Li, x, t_{irr})$ is the number of transmuted atoms at the position x in the pellet and at the irradiation duration t_{irr}.

The estimated maximum thermal gradient is about 5×10^{-3} K m^{-1}. This value is very weak and the temperature along the radius of the sample is considered as constant and equal to 773 K. At this temperature, no lithium compounds are created.

The second possibility is the formation of inter or intra granular lithium inclusions. Copeland et al. have irradiated boron carbide sample in a thermal flux spectrum and examined slides of irradiated boron carbide by transmission electron microscopy. They did not find any lithium precipitates [12]. From these studies, we deduce that no lithium precipitates are created in the boron carbide sample.

The third and most probable possibility is a ^{7}Li solubility in the boron carbide lattice. The unit cell of boron carbide is rhombohedral with icosahedral units on the corners and three atom chain along the main diagonal. In this structure lithium atoms may be in interstitial position in the lattice. Lithium atoms may diffuse in atomic form through the grains or the grain boundaries into pores [13].

According to the thermodynamics of irreversible processes, the flux of lithium atoms depends on the temperature and on the number of lithium atoms per unit volume according to the following relation [14]:

$$J_{Li} = -D_{Li} \nabla N(Li) - \frac{N(Li) D_{Li}}{kT(x)} Q_B \frac{\nabla T(x)}{T(x)}; \quad (8)$$

Q_B is the apparent heat of transport (J), D_{Li} is the lithium diffusion coefficient in the boron carbide (m^2 s^{-1}), and k is the Boltzmann constant (J K^{-1}).

As has been shown before (Eq. (6)), the temperature gradient is weak (5×10^{-3} K m^{-1}) and then the lithium flux depends only on the lithium atoms gradient.

The lithium diffusion takes place not only in the grain but also in the grain boundary. However, the grain boundary diffusion is assumed to be much more rapid than intragranular diffusion. For this reason, the choice of geometry for grain boundary diffusion is not discussed. The limiting step is only the lithium diffusion in the boron carbide grain.

4.1.2. Desorption at the solid pore interface

At the solid phase pore interface, lithium atoms desorb into pores. The simplest lithium desorption model is the Langmuir mechanism. The lithium release rate, R, in a first order desorption reaction is given by

$$R(t) = \frac{-dC_s}{dt} = k_0 C_s \exp\left(-\frac{E_{des}}{kT}\right); \quad (9)$$

C_s is the number of lithium atom per surface unit (atoms m^{-2}), k_0 is the pre-exponential factor (s^{-1}), E_{des} is the desorption energy (J), T is the temperature (K), and k is the Boltzmann constant (J K^{-1}).

This desorption mechanism occurs while the lithium partial pressure in each pore is lower than the lithium saturated vapor pressure.

4.1.3. Migration through pores

The high level of interconnected porosity (23.3%) allows to think that lithium gas atoms can migrate through pores out of the pellet in the capsule free volume. The lithium flux in pores is given by

$$J_{Li} = -D_{eff} \nabla N^g(Li); \quad (10)$$

$N^g(Li)$ is the number of lithium gas atoms in pores (atoms m^{-3}) and D_{eff} is the effective diffusion coefficient (m^2 s^{-1}).

his coefficient can be estimated [15]. It depends on pore tortuosity, pore size, pore distribution and on the lithium diffusion coefficient in helium (helium fills interconnected pores in the pellet). The tortuosity factor is used to account for the fact that the diffusive path length is longer than the physical dimension of the porous material. The pore size distribution induces constrictions and expansions which modify speed of lithium gaseous atoms. The lithium effective diffusion coefficient in pores is many orders of magnitude higher than the lithium diffusion coefficient in a boron carbide grain.

This interpretation can not be actually quantified. More information is needed:

- Li diffusion coefficient in boron carbide grain,
- lithium desorption coefficient at the surface,
- detailed information on pores (arrangement, shape, diffusion coefficient),
- possibility of the formation of lithium compounds under irradiation.

To obtain these data, different experimental techniques would be used like nuclear microanalysis, specific surface

BET, Raman spectroscopy. These different approaches are under development.

4.2. Ejection of lithium atoms at the sample surface

At the surface of the pellet, another mechanism contributes to the lithium migration out of the sample. Lithium atoms produced by the $^{10}B(n, \alpha)^{7}Li$ reaction have a mean energy of 0.83 MeV. It corresponds to a path length of about 1.7 μm in boron carbide which is the same order of magnitude as grain size. A lithium atom produced in the two first μm from the surface of the sample can leave the grain and go out of the pellet.

The lithium migration out of the sample stops only when the lithium partial pressure in the capsule free volume is equal to the lithium saturated vapor pressure.

5. Conclusion

The experimental ^{10}B profile is in good agreement with the calculated ^{10}B distribution deduced from a classical neutron absorption mechanism. It implies that there is no migration of ^{10}B in the irradiated boron carbide pellet.

A ^{7}Li profile has been calculated from the experimental ^{10}B distribution and compared to the experimental data. A large discrepancy of about 40% is observed. We suggest a ^{7}Li desorption out of the grain followed by a migration through pores to the capsule free volume. This qualitative interpretation has to be confirmed by a quantitative study. Different experimental approaches are suggested to define all the parameters needed to propose a lithium migration explanation from the grain to the outside of the pellet.

The ^{7}Li migration out of the boron carbide pellet leads to a relative mass variation of about 6×10^{-3}, which is not very significant in the present case. In FBR or for longer irradiation times in PWR, this relative mass variation can become more important. It may contribute to the swelling of boron carbide absorbers. The actual calculations of the swelling based on a density variation method including only the helium production, must take into account this lithium migration.

In addition, during the neutron irradiation in a PWR, the lithium lost from the pellet may settle on the metallic sheath holding the pellets and migrate inside the sheath inducing its brittleness.

References

[1] T. Stoto, L. Zuppiroli and J. Pelissier, Radiat. Eff. 90 (1985) 161.
[2] J.W. McMillan, F.C.W. Pummery and P.M. Pollard, Nucl. Instrum. Meth. 197 (1982) 171.
[3] Ch. Engelmann and G. Revel, Nucl. Instrum. Meth. B554 (1991).
[4] J.F. Ziegler, Handbook of Stopping Power of Energetic Ions in All Elements, Vol. 5 (Pergamon).
[5] W.H. Bragg and R. Kleeman, Philos. Mag. 10 (1905) 5318.
[6] R. Jarjis, PhD thesis, University of Manchester (1979).
[7] C. Olivier and M. Peisach, J. Radioanal. Chem. 98 (1986) 389.
[8] D.E Mahagin, L.L. Bates and D.E. Baker, Report HELD-TME/77-33 (1977).
[9] D.R. Secrist, J. Am. Ceram. Soc. 50 (10) (1967) 520.
[10] F.E. Wang, M.A. Mictchell, R.A. Sutula, J.R. Holden and L.H. Bennett, J. Less-Common Met. 61 (1978) 237.
[11] A.R. Raffray, S. Cho and M.A. Abdou, J. Nucl. Mater. 210 (1994) 143.
[12] G.L. Copeland, R.G. Donnelly and W.R. Martin, Nucl. Technol. 16 (1972) 226.
[13] B. Rasner, CEA/CEREM ref. NT 94/014 BR/FL (1994).
[14] J. Bocquet, G. Brebec and Y. Limoge, in: Physical Metallurgy, eds. R.W. Cahn and P. Haasen (Elsevier Science, Amsterdam, 1996), p. 543.
[15] G. Federici, A.R. Raffray and M.A. Abdou, A Comprehensive Model for Tritium Transport in Lithium Base Ceramics, Vol. 173 (1990) pp. 214–228.